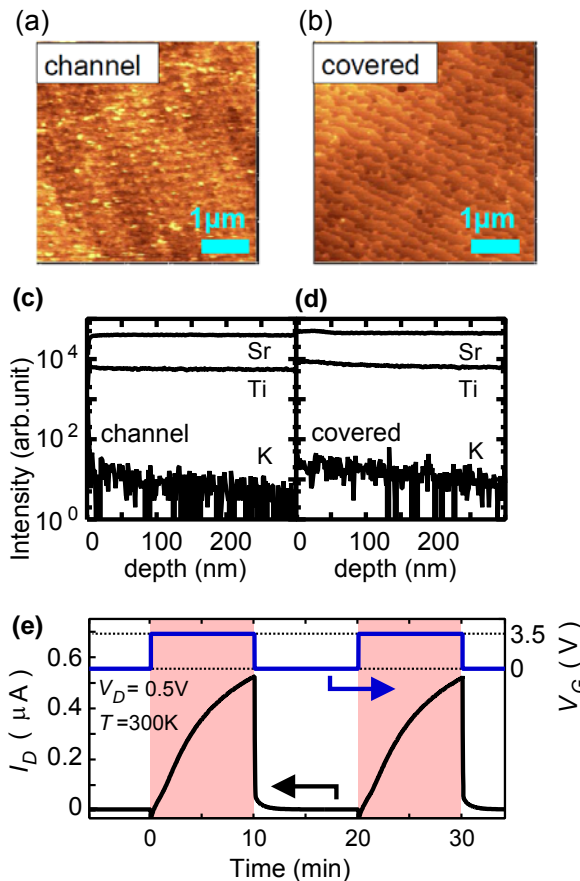


# Supplementary Information

## 1. Confirmation of no chemical reactions during the FET measurements

In order to confirm that any possible electrochemical reaction did not damage the SrTiO<sub>3</sub> crystal surface during the measurement, the channel surface was examined by atomic force microscopy (AFM) and secondary ion mass spectroscopy (SIMS) after the electrical measurements. The sample was identical to that used for observing superconductivity while cooling down to low temperatures several times with applying bias voltages. Polymer electrolyte and separator film on the sample were removed after measurements. An AFM image of the surface after the measurement shows a clear step and terrace structure as shown in Fig. S1 (a) similar to the area covered by the separator film (Fig. S1 (b)) as well as that of an original SrTiO<sub>3</sub> single crystal. There was no contrast seen at the boundary between the channel area and the covered area. Therefore, it is unlikely to have induced any reaction such as etching. In Fig. S1 (c) and S1 (d), the depth profiles of Sr, Ti and K ions in SIMS measurements are shown for the channel and covered areas, respectively. The signal level for K is similar for both cases and is close to the detection limit. Therefore, we can conclude that there is no detectable intercalation of K ions into SrTiO<sub>3</sub> crystal that might donate electrons into SrTiO<sub>3</sub>.



**Figure S1** Atomic force microscope (AFM) images for the surfaces of the channel after repeated FET measurements (a) and that for the area covered by separator film (b). Depth profiles of secondary ion mass spectroscopy for the channel (c) and the covered areas (d). (e) Switching characteristics of the EDLFET device between  $V_G=0$  V and 3.5 V.

Merely from the AFM and SIMS results, we cannot exclude an electrochemical reduction of SrTiO<sub>3</sub> for donating oxygen vacancy that will also work as electron donors. We show a temporal profile of  $I_D$  while  $V_G$  was switched between 0 V (off) and 3.5 V (on) at 10 minutes intervals with applying  $V_D=0.5$  V at 300 K. As shown in Fig. S1 (e), it took more than 10 minutes to attain saturation of  $I_D$  when switch-on but  $I_D$  quickly dropped by 90% for 5 seconds and a slight decay emerged for a few minutes to reach almost zero current. The gradual switching-on is presumably due to a low cation mobility in the electrolyte. Since the effective thickness of the electric double layer is reduced by the collection and closed-pack arrangement of cations, slow motion of cations will gradually increase an effective electric field. However, the removal of  $V_G$  rapidly destroys the electric double layer within 5sec even though cations exist nearby the channel. If the conduction of the channel were originated by oxygen vacancy diffused into the channel, the device would show slow switching-off with similar time constant due to low diffusion constant of oxygen vacancies in SrTiO<sub>3</sub> crystal at 300K. Therefore, the rapid switching-off of the device evidences that the oxygen vacancy is not the origin.

## 2. Comparison with conductive interface at LaAlO<sub>3</sub>/SrTiO<sub>3</sub>

The relevance of the metallic conduction in the SrTiO<sub>3</sub> channel of our EDLFET is examined to the conductive interface formed by growing thin LaAlO<sub>3</sub> layers on SrTiO<sub>3</sub> substrates. Figure S2 shows relationship between sheet charge density  $n_{2D}$  and mobility  $\mu_H$  at around 2 K for our results as well as the ones reported for LaAlO<sub>3</sub>/SrTiO<sub>3</sub> interfaces from various groups. The relationship between volume charge density  $n_{3D}$  and  $\mu_H$  in bulk SrTiO<sub>3</sub> single crystals was also plotted for comparison. We found that most of the data can be classified into three groups, denoted by A, B and C in Fig. S2.

Group A has  $n_{2D}$  ranging from  $10^{13}$  to  $10^{14}$  cm<sup>-2</sup> and  $\mu_H$  of around  $10^3$  cm<sup>2</sup>/Vs. This group includes superconducting interfaces of LaAlO<sub>3</sub>/SrTiO<sub>3</sub>(Ref.1). The relationship between  $n_{2D}$ - $\mu_H$  shows good correspondence to that of bulk data with an assumption that the thickness of the conductive layer is 10 nm. In addition, the samples showing superconductivity have weakly temperature dependent  $R_H$  from 300 K and 4.2 K suggesting that oxygen vacancies in the substrate are not responsible for the conduction in this group. Therefore, conduction in this group is probably quasi-two-dimensional and confined within several nm. Most of our results are included in this group. Group B has  $n_{2D}$  ranging from  $10^{13}$  to  $10^{15}$  cm<sup>-2</sup> and  $\mu_H$  smaller than  $10$ cm<sup>2</sup>/Vs. This group includes ferromagnetic interfaces between LaAlO<sub>3</sub>/SrTiO<sub>3</sub> and ones showing unusual increase of sheet resistance at low temperature<sup>2</sup>. Group C has  $n_{2D}$  above  $10^{16}$  cm<sup>-2</sup> and  $\mu_H$  of around  $10^4$  cm<sup>2</sup>/Vs. This group includes ones showing oscillating

magnetoresistance<sup>3</sup>. Herranz *et al.* concluded that three dimensional SdH oscillations took place in a conductive layer as thick as 530  $\mu\text{m}$  that is identical to the thickness of a substrate<sup>4</sup>. Accordingly, conduction in this group may be mainly induced from high density of oxygen vacancies in the substrate.

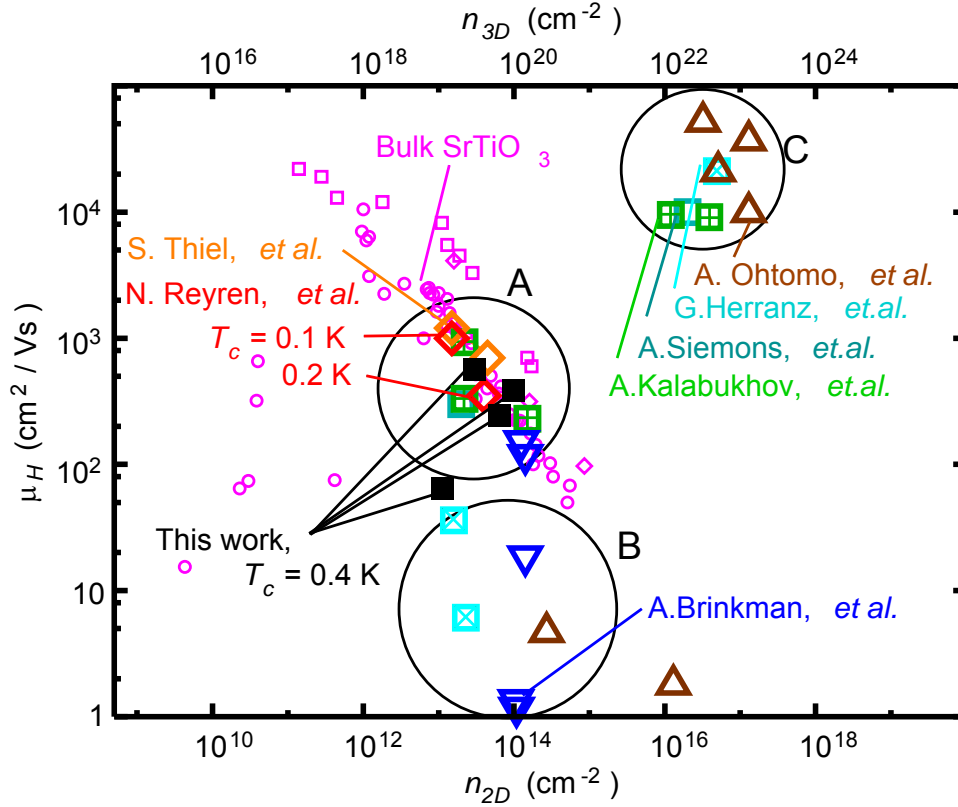


**Figure S2** Relationship between Hall mobility  $\mu_H$  and sheet charge density  $n_{2D}$  in this work (black solid squares) as well as those for  $\text{LaAlO}_3/\text{SrTiO}_3$  interfaces reported from various groups. The latter include superconducting<sup>1</sup> (red open diamonds), ferromagnetic<sup>2</sup> (blue open triangles), oscillating magnetoresistance<sup>3</sup> (brown triangles), and others (dark cyan boxes<sup>4</sup>, open red diamonds<sup>5</sup>, dark pink boxes<sup>6</sup>, green boxes<sup>7</sup>). Top axis shows corresponding volume charge density  $n_{3D}$  with an assumption that thickness of the conducting layer is 10 nm. Relationship between  $\mu_H$  and  $n_{3D}$  for bulk single crystals is also shown for comparison by small pink circles, boxes and diamonds for those doped with oxygen vacancy, Nb, and La, respectively<sup>8-12</sup>. Three circles(A,B, and C) denotes the three groups of  $\text{LaAlO}_3/\text{SrTiO}_3$  interfaces (discussed in text).

### 3. Calculation methods and subband structures for the accumulation layer of SrTiO<sub>3</sub>

We calculated the subband structure with a triangular potential approximation<sup>13</sup>. In this approximation, the confinement potential was given by an infinite barrier at  $z < 0$  and by  $V(z) = eF_{av}z$  for  $z > 0$ , where  $F_{av}$  is an average electric field. When a relative dielectric constant  $\epsilon_r$  in a semiconductor channel is independent of an electric field,  $F_{av}$  is given by  $0.5en_{2D}/\epsilon_0\epsilon_r$ . When  $\epsilon_r$  depends on the electric field,  $F_{av}$  is an analytical solution of

$$0.5en_{2D} = \int_0^{F_{av}} \epsilon_0 \epsilon_r(F) dF. \quad (1)$$

The field dependence of  $\epsilon_r$  in SrTiO<sub>3</sub> has been reported as

$$\epsilon_r(F) = \frac{1}{A + BF}, \quad (2)$$

where  $F$  is an electric field,  $\epsilon_0$  is 8.85 pF/m,  $A$  and  $B$  are  $4.097 \times 10^{-5}$  and  $4.907 \times 10^{-10}$  m/V, respectively, at 4.2 K (ref. 14). One can deduce  $F_{av}$  as

$$F_{av} = \frac{A}{B} \left( \exp\left(\frac{B}{\epsilon_0} 0.5n_{sheet}\right) - 1 \right). \quad (3)$$

The solutions of the Schrödinger equation with a triangular potential approximation are Airy functions,

$$\zeta_i(z) = Ai \left[ \frac{z}{z_0} - \frac{E_i}{eF_{av}z_0} \right], \quad i = 1, 2, 3, \dots \quad (4)$$

and

$$z_0 = \left( \frac{\hbar^2}{2m^* eF_{av}} \right)^{1/3}, \quad (5)$$

where  $m^*$  is an effective mass for the motion along with the confinement potential, and the eigen values  $E_i$  are given by

$$E_i \sim eF_{av}z_0 \left[ \frac{3\pi}{2} \left( i - \frac{1}{4} \right) \right]^{2/3}. \quad (6)$$

SrTiO<sub>3</sub> was reported to have three doubly-degenerated conduction band valleys centered at  $\Gamma$  point with their long axis along [100], [010] and [001] directions<sup>15</sup>. Band calculations proposed that the bands are split to three doubly-degenerated bands due to spin-orbit interaction and tetragonal distortion of SrTiO<sub>3</sub> below 100 K with splitting energies of 20meV and 100meV, respectively<sup>16</sup>, while Shubnikov-de Hass (SdH) effect experiments showed that there are two bands with a splitting energy of 1.5meV (ref. 17). In this calculation, we

assumed that there was no band-splitting in the three bands, since the splitting energy is not conclusively determined. Each valleys have a longitudinal effective mass  $m_l^*$  of  $4.8m_0$  and a transverse effective mass  $m_t^*$  of  $1.2m_0$ , where  $m_0$  being free electron mass. With a definition of [001] as the direction of the confinement potential, one valley along [001] direction has the heavier effective mass  $m_l^*$  and lower values of  $E_i$  than those of other two valleys. Each subbands have a constant density of states equal to  $gm^*/2\pi\hbar^2$ , where  $g$  is a valley degeneracy factor. The Fermi energy  $E_F$  is numerically deduced so that total charge density equals to  $n_{2D}$ . Depth profile of the accumulation layer is given by summing the charge density of each subband of the valley with light and heavy effective masses, as

$$n_{3D}(z) = g_l \frac{m_l^*}{2\pi\hbar^2} \sum_i (E_F - E_{li}) |\zeta_{li}(z)|^2 + g_h \frac{m_h^*}{2\pi\hbar^2} \sum_i (E_F - E_{hi}) |\zeta_{hi}(z)|^2, \quad (7)$$

where the valley degeneracy factors  $g_l$  and  $g_h$  are 4 and 2, respectively, and  $\zeta_{li}$  and  $\zeta_{hi}$  are the normalized wave functions of the  $i$ -th subband for the valleys with the light and heavy effective masses, respectively. Mean depth  $\langle d \rangle$  and mean volume charge density  $\langle n_{3D} \rangle$  were given by

$$\langle d \rangle = \int z n_{3D}(z) dz / \int n_{3D}(z) dz, \quad (8)$$

and

$$\langle n_{3D} \rangle = \int n_{3D}^2(z) dz / \int n_{3D}(z) dz. \quad (9)$$

Figure S3 (a) shows the subband structures of the two dimensional electron gas in SrTiO<sub>3</sub> deduced from  $n_{2D}$  at various gate biases  $V_G$ . Density of states (*DOS*) in a three dimensional case is also schematically drawn in Fig. S3 (b) for comparison. Two dimensional *DOS* at  $E_F$  is nearly independent of  $V_G$  with a slightly decrease with increasing  $V_G$  due to the enhanced confinement potential. In contrast, three dimensional *DOS* was monotonically increased with increased charge density. The subband structure is insignificantly changed down to  $n_{2D}=10^{11}/\text{cm}^2$ , while  $E_F$  decreases below 0.1meV, whereas number of occupied subbands was decreased with increasing  $n_{2D}$  above  $1 \times 10^{14} \text{cm}^{-2}$ . Only the lowest subband was occupied when  $n_{sheet}$  was at above  $2 \times 10^{14}$  due to the reduction of  $\epsilon_r$  to 3.3 and enhancement of  $F_{av}$  to 0.6MV/cm. Figure S3 (c) shows relationship between superconducting transition temperature  $T_c$  and mean volume charge density  $\langle n_{3D} \rangle$ . The data for superconducting interfaces of LaAlO<sub>3</sub>/SrTiO<sub>3</sub> (red open diamonds) and bulk SrTiO<sub>3-x</sub> single crystals (small open circles) are also shown for comparison<sup>2,13</sup>, for which  $\langle n_{3D} \rangle$  of the LaAlO<sub>3</sub>/SrTiO<sub>3</sub> was estimated with an assumption of 10nm thick conducting layer. The value of  $T_c$  for this work (black solid squares) is virtually independent of  $\langle n_{3D} \rangle$  that is very distinct from the bulk and the LaAlO<sub>3</sub>/SrTiO<sub>3</sub> interface superconductivity. Here we note that Fig. S3 (c) alone may be

misleading and one need to consider that there is considerable distributions in local  $n_{3D}$  along depth as shown in Fig. S3 (d). Nonetheless, it is clear that peak  $n_{3D}$  hardly approaches the carrier density needed for attaining maximum  $T_c$  in bulk SrTiO<sub>3</sub> under relatively low  $V_G$  of 2.5 and 2.7V.

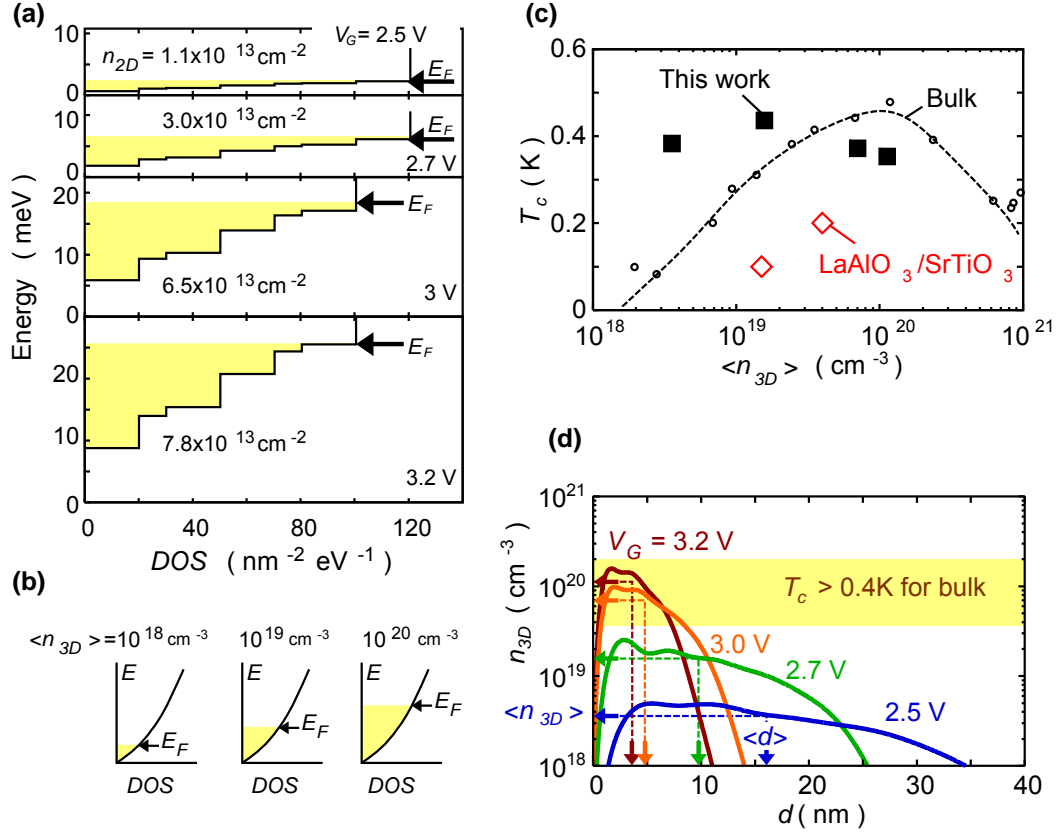


**Figure S3 (a)** Density of states (DOS) as a function of energy  $E$  deduced for various gate biases.  $E_F$  denotes the Fermi energy. DOS at  $E_F$  is virtually unchanged with increasing  $V_G$ . **(b)** Schematics of DOS- $E$  relationship in a three dimensional case. DOS at  $E_F$  is monotonically increased with the charge density  $n_{3D}$ . **(c)** Relationship between transition temperature  $T_c$  and volume charge density  $n_{3D}$  deduced from the calculation for this work (black solid squares). For comparison, the data for superconductive LaAlO<sub>3</sub>/SrTiO<sub>3</sub> interfaces and bulk SrTiO<sub>3-x</sub> single crystals are shown as red diamonds and small circles with dotted line, respectively<sup>2,18</sup>. **(d)** Depth profile of  $n_{3D}$  calculated by Eq. 7 for various  $V_G$ . Also indicated are the weighted mean values of carrier distribution depth  $\langle d \rangle$  and volume charge density  $\langle n_{3D} \rangle$  calculated from Eqs. 8 and 9, respectively.

## References

- 1 Brinkman, A., Huijben, M., Van Zalk, M., Huijben, J., Zeitler, U., Maan, J. C., Van Der Wiel, W. G., Rijnders, G., Blank, D. H. A. & Hilgenkamp, H. Magnetic effects at the interface between non-magnetic oxides, *Nature Mater.* **6**, 493-496 (2007).
2. Reyren, N., Thiel, S., Caviglia, A. D., Kourkoutis, L. F., Hammerl, G., Richter, C., Schneider, C. W., Kopp, T., Rüttschi, A.-S., Jaccard, D., Gabay, M., Muller, D. A., Triscone, J.-M. & Mannhart, J. Superconducting Interfaces Between Insulating Oxides, *Science* **317**, 1196-1199 (2007).
3. Ohtomo, A. & Hwang, H. Y. A high-mobility electron gas at the LaAlO<sub>3</sub>/SrTiO<sub>3</sub> heterointerface, *Nature* **427**, 423-426 (2004).
- 4 Herranz, G., Basletić, M., Bibes, M., Carrétéro, C., Tafrá, E., Jacquet, E., Bouzehouane, K., Deranlot, C., Hamzić, A., Broto, J.-M., Barthélémy, A. & Fert, A. High Mobility in LaAlO<sub>3</sub> / SrTiO<sub>3</sub> Heterostructures: Origin, Dimensionality, and Perspectives, *Phys. Rev. Lett.* **98**, 216803 (2007).
- 5 Thiel, S., Hammerl, G., Schmehl, A., Schneider, C. W. & Mannhart, J. Tunable Quasi-Two-Dimensional Electron Gases in Oxide Heterostructures, *Science* **313**, 1942-1945 (2006).
- 6 Siemons, W., Koster, G., Yamamoto, H., Harrison, W. A., Lucovsky, G., Geballe, T. H., Blank, D. H. A. & Beasley, M. R. Origin of Charge Density at LaAlO<sub>3</sub> on SrTiO<sub>3</sub> Heterointerfaces: Possibility of intrinsic doping, *Phys. Rev. Lett.* **98**, 196802 (2007).
- 7 Kalabukhov, A., Gunnarsson, R., Börjesson, J., Olsson, E., Claeson, T. & Winkler, D. Effect of oxygen vacancies in the SrTiO<sub>3</sub> substrate on the electrical properties of the LaAlO<sub>3</sub> / SrTiO<sub>3</sub> interface, *Phys. Rev. B* **75**, 121404 (2007).
- 8 Koonce, C. S., Cohen, M. L., Schooley, J. F., Hosler, W. R. & Pfeiffer, E. R. Superconducting Transition Temperatures of Semiconducting SrTiO<sub>3</sub>, *Phys. Rev.* **163**, 380-390 (1967).
- 9 Frederikse, H. P. R., Thurber, W. R. & Hosler, W. R. Electronic Transport in Strontium Titanate, *Phys. Rev.* **134**, A442-A445 (1964).
- 10 Lee, C., Yahia, J. & Brebner, J. L. Electronic Conduction in Slightly Reduced Strontium Titanate at Low Temperature, *Phys. Rev. B* **3**, 2525-2533 (1971).
- 11 Moos, R., Menesklou, W. & Härdtl, K. H. Hall mobility of undoped n-type conducting strontium titanate single crystals between 19K and 1373K, *Appl. Phys. A* **61**, 389-395 (1995).
- 12 Tufte, O. N. & Chapman, P. W., Electron Mobility in Semiconducting Strontium Titanate, *Phys. Rev.* **155**, 796-802 (1967).
13. Ando, T., Fowler, A. B. & Stern, F. Electronic properties of two-dimensional systems,

*Rev. Mod. Phys.* **54**, 437-672 (1982).

14 Neville, R. C., Hoeneisen, B. & Mead, C. A. Permittivity of Strontium Titanate, *J. Appl. Phys.* **43**, 2124-2131 (1972).

15 Mattheiss, L.F. Energy Bands for  $\text{KNiF}_3$ ,  $\text{SrTiO}_3$ ,  $\text{KMoO}_3$ , and  $\text{KTaO}_3$ , *Phys. Rev. B.* **6**, 4718-4740 (1972).

16 Mattheiss, L.F. Effect of 110°K Phase Transition on the  $\text{SrTiO}_3$  Conduction Bands, *Phys. Rev. B*, **6**, 4740-4753 (1972).

17 Uwe, H., Yoshizaki, R., Sakudo, T., Izumi, A. & Uzumaki, T. Conduction Band Structure of  $\text{SrTiO}_3$ , *Jpn. J. Appl. Phys.* **24**, Suppl **24-2**, 335-337 (1985).

18 Schooley, J. F., Hosler, W. R., Ambler, E., Becker, J. H., Cohen, M. L. & Koonce, C. S. Dependence of the superconducting transition temperature on carrier concentration in semiconducting  $\text{SrTiO}_3$ , *Phys. Rev. Lett.* **14**, 305-307 (1965).